S-layer protein-AuNP systems for the colorimetric detection of metal and metalloid ions in water

J. Jung[a,*,1], M. Lakatos[b,1], S. Bengs[c], S. Matys[d], J. Raff[e], A. Blüher[f,*], G. Cuniberti[a]

[a] Institute for Materials Science and Max Bergmann Center of Biomaterials, TU Dresden, 01062, Dresden, Germany
[b] Photonic Nanosystems, Department of Physics, University Fribourg, 1700, Fribourg, Switzerland
[c] Department of Nuclear Medicine, Cardiovascular Gender Medicine, University Hospital Zurich, Switzerland
[d] Helmholtz-Institute Freiberg for Resource Technology, Chemnitzer Str. 40, 09599, Freiberg, Germany
[e] Helmholtz-Zentrum Dresden Rossendorf, Institute of Resource Ecology, Bautzner Landstraße 400, 01328, Dresden, Germany
[f] School of Engineering Science, TU Dresden, 01062, Dresden, Germany

ARTICLE INFO

Keywords:
S- layer
Gold nanoparticles
Colorimetric assay
Rare earth elements

ABSTRACT

Bacterial surface layer proteins (S-layer) possess unique binding properties for metal ions. By combining the binding capability of S-layer proteins with the optical properties of gold nanoparticles (AuNP), namely plasmonic resonance, a colorimetric detection system for metal and metalloid ions in water was developed. Eight S-layer proteins from different bacteria species were used for the functionalization of AuNP. The thus developed biohybrid systems, AuNP functionalized with S-layer proteins, were tested with different metal salt solutions, e.g. Indium(III)-chloride, Yttrium(III)-chloride or Nickel(II)-chloride, to determine their selective and sensitive binding to ionic analytes. All tested S-layer proteins displayed unique binding affinities for the different metal ions. For each S-layer and metal ion combination markedly different reaction patterns and differences in concentration range and absorption spectra were detected by UV/vis spectroscopy. In this way, the selective detection of tested metal ions was achieved by differentiated analysis of a colorimetric screening assay of these biohybrid systems. A highly selective and sensitive detection of yttrium ions down to a concentration of 1.67×10^{-5} mol/l was achieved with S-layer protein *SslA* functionalized AuNP. The presented biohybrid systems can thus be used as a sensitive and fast sensor system for metal and metalloid ions in aqueous systems.

1. Introduction

Most surface layer protein (S-layer) bearing bacteria survive in extreme environmental conditions, such as high temperature, strong acidic surroundings, high salt concentrations, or high pressure. Therefore it is assumed the S-layer proteins primarily serves as protection against the environment. Those microorganisms have developed various mechanisms for this purpose, including dealing with toxic metals by binding them to their S-layer [1–4]. S-layers form the outermost structures of these bacteria and archaea. They consist of subunits of identical (glyco-) proteins that can self-assemble into highly ordered crystalline structures of varying symmetries with pores of 2–8 nm and a thickness of 5–15 nm [5,6]. Studies revealed unique and characteristic affinities for different metal and metalloid ions for S-layer species [7–10]. These natural binding properties, originated by the evolutionary development, can be used for a wide variety of nanotechnological applications [11–15], e.g. for the development of water treatment systems or for the recovery of valuable metals from water [16].

Moreover, the metal-binding properties of S-layer proteins can be used in a broad range of sensing applications. One example of such a sensing platform is the arsenic sensing in water using colloidal AuNP functionalized with the S-layer protein of *Lysinibacillus sphaericus* JG-A12 [17]. Contaminant (bio) monitoring and assessment of valuable elements or pollutants in an aqueous environment has become increasingly important for both environmental protection and commercial applications. Notably, the ability to detect rare-earth elements has growing significance over the past few years, also due to their widespread incorporation in electronic devices [18,19].

Metallic compounds enter the aqueous systems of the environment by means of mining and industrial production processes, as well as by natural weathering processes. This entry of pollution has become an increasing problem within the recent years and affected the living conditions of organisms, as well as human health [20–26]. The

* Corresponding authors.
E-mail addresses: jonas.jung@tu-dresden.de (J. Jung), anja.blueher@tu-dresden.de (A. Blüher).
[1] Equally contributed.

detection of heavy metals in water using biological markers poses certain challenges: Variations in species composition, conditions at sampling sites, differences in seasonal sampling, and age of organism, as well as different metal levels in different parts of the organism, make the interpretation of results difficult [27]. This underlines the importance of the development of fast and precise detection methods for such elements.

Established systems for the identification of these metal and metalloid ions can be divided into two groups. The first group is highly sensitive and can detect a broad range of analytes and includes e.g. high performance liquid chromatography, inductively coupled plasma atomic emission spectroscopy, and inductively coupled plasma time-of-flight mass spectrometry [28–31]. The drawbacks of such methods are: they are very expensive, time consuming, and often require special sample preparation. The second group involves the use of specialized test kits. This approach utilizes characteristic chemical reactions, and results can be analyzed by UV/Vis spectroscopy, fluorescence measurements, or even visually [32]. Although they provide fast results, these tests are limited by design to detect only one specific analyte based on a particular reaction type. The development of novel bio-based materials for the detection of metal and metalloid ions offers new screening tools, which will overcome these limitations. In particular, biohybrid materials show great promise due to a range of advantageous characteristics associated with the combination of inorganic and biological-derived materials [33]. The aim of our investigation was to assess the behavior of different S-layer-functionalized AuNP systems with a variety of ions or ionic complexes of noble and rare-earth metals, in order to test their suitability in sensor applications in an aqueous environment.

2. Materials and methods

All solutions were prepared with ultrapure water (MembraPure, electrical conductivity ≤ 0,055µS).

2.1. AuNP synthesis and characterization

Spherical AuNP with 20–30 nm in diameter were synthesized using the adapted Turkevich-Method [34,35]. The volume of 2 ml trisodiumcitrate trihydrate solution ($C_6H_5Na_3O_7{\cdot}2H_2O$, 3.4×10^{-2} mol/l) was added to a continuously stirring solution of 100 ml chloroauric acid ($HAuCl_4{\cdot}3H_2O$; 0.5×10^{-3} mol/l) at 100 °C. Within a few minutes the color changed from slight yellow to dark blue, before turning burgundy, indicating the formation of a colloidal solution of spherical AuNP. To complete the reaction, heating and stirring was continued for one hour. To prevent particle agglomeration by evaporation of the solvent, the amount of water (100 ml) was always kept constant during the whole process, by manually adding the proper amount.

The absorption of the colloidal AuNP solutions was measured with a Varian Cary 100 UV/Vis spectrophotometer (Varian Inc., Canterbury, Australia). Scanning electron microscopy (SEM, LEO 982 Gemini, LEO Elektronenmikroskopie GmbH, Oberkochen, Germany) and transmission electron microscopy (TEM, Zeiss Libra 200, Zeiss Oberkochen, Germany) were used to determine the size and shape of the AuNP.

2.2. S-layer protein extraction and AuNP functionalization

The extraction of the eight different S-layer proteins was carried out as described by Blüher et al. 2015 with slight modifications [36]. The bacteria species *Lysinibacillus fusiformis* DSMZ 2898, *Lysinibacillus sphaericus* JG-A12 (SlfB), *Lysinibacillus sphaericus* JG-B53 (Slp1), *Lysinibacillus sphaericus* JG-B62, *Lysinibacillus sphaericus* NCTC 9602 (SlfA) and *Sporosarcina ureae* ATCC 13881 (SslA) were grown for 17–20 h under aerobic conditions in liquid medium (5 g/l BactoTMPeptone, Becton, Dickinson and Company, Sparks, USA, and 3 g/l meat extract, Merck, Germany) at 30 °C. Two bacteria species are thermophilic, *Geobacillus stearothermophilus* ATCC 12980 (SbsA) and *Thermoanaerobacterium thermosulfurigenes* EM1. Therefore, they were grown at a higher temperature of 60 °C. Additionally *T. thermosulfurigenes* EM1 was grown under anaerobic conditions [37,38].

S-layer oligomeric solutions were obtained by disassembling the crystalline S-layer fragments (tubes or sheets) in suspension with 6 mol/l guanidine hydrochloride, followed by centrifugation at 14,000*g* for 30 min at 4 °C and a subsequent dialysis against 0.5×10^{-3}mol/l TRIS buffer. The oligomer solutions were stored at 4 °C.

The biofunctionalization of AuNP with S-layer proteins was done by adsorption processes. In a first step, the concentration of required S-layer proteins to stabilize the AuNP was assessed by mixing a series of 50 µl S-layer proteins of decreasing concentration (from 1–0.001 mg/ml) with a constant amount of 100 µl AuNP (OD_{523} = 1; absorbance maximum of 1 at 523 nm). For protein adsorption to the gold surfaces, the mixtures were incubated for 10 min at RT. After 10 min 10 µl of a 10% sodium chloride solution (NaCl) were added, to check the stability of the formed biohybrid nanoparticles. By this so called salt test [39], insufficient stabilized nanoparticles tend to agglomerate, indicated by a color change of the AuNP solution from red to blue or purple within 5–10 min after adding NaCl. For the following analytical experiments, in principle the lowest required S-layer concentration, which still produces a stable biohybrid AuNP solution, was used. No differences in reaction time for the adsorption of different S-layer proteins with the AuNP were observed (see Supplementary information, Fig. SI1).

In the second step, the volume of the AuNP solution with the estimated S-layer protein concentration from step one for the functionalization was scaled up. Therefore, 10 ml of an AuNP solution (20–30 nm size, OD_{523} = 1) were incubated with the calculated appropriate concentration of S-layer protein for at least 6 h. To achieve a full saturation of the nanoparticle surface with the protein, very careful shaking was applied. To eliminate unbound protein from the biofunctionalized AuNP, the suspension was centrifuged 2–3 times at 4 °C for 30 min at 3000*g*. The supernatant was carefully removed and the pellet resuspended in 0.1% polyvinyl alcohol (PVA) until a final OD_{525} = 1 was achieved and the nanoparticles received an enhanced stability by addition of this short polymer. The subsequent biofunctionalized AuNP solutions shows a red color and were characterized by UV/Vis spectroscopy and TEM imaging (the latter using WSXM software) [40].

2.3. Metal salt detection by colorimetric screening with S-layer-AuNP systems

In an experiment, 100 µl of S-layer functionalized AuNP (OD_{525} = 1) were mixed with 50 µl of a metal salt solution of Yttrium (III)-chloride (YCl_3), Copper(II)-sulfate ($CuSO_4$), Indium(III)-chloride ($InCl_3$), Potassium tetrachloroplatinate(II) (K_2PtCl_4), Gold(III)-chloride ($HAuCl_4$), Holmium(III)-nitrate ($Ho(NO_3)_3$), Samarium(III)-nitrate ($Sm(NO_3)_3$), Gallium(III)-nitrate ($Ga(NO_3)_3$), Copper(II)-nitrate ($Cu(NO_3)_2$), Sodium-hydrogen-arsenate(V) (Na_2HAsO_4) or Nickel(II)-chloride ($NiCl_2$). This was repeated for a series of dilutions in a concentration range of 0.08–0 mol/l of the analyte. To define the baseline values of the experimental series for the specific biohybrid-systems and analytes, the same experiments were carried out with non-functionalized AuNP, which were stabilized by 0.1% PVA (OD_{525} = 1).

Analyte detection was achieved by monitoring the color change of the solution, which occurred within the first 5 min. These color changes are based on the agglomeration of the functionalized AuNP and were quantified by UV/Vis absorption spectra analysis of the solutions with a Tecan Infinite 200 Pro plate reader (Tecan Group AG, Männedorf, Switzerland).

2.4. Comparison of protein sequences using the universal protein database (UniProt)

To investigate the genetic similarity of the S-layer proteins, the

UniProt database was employed [41–43]. In order to compare two protein sequences, the sequence data in FASTA format were analyzed with a NCBI Standard basic local alignment search tool (BLAST). BLAST is an algorithm used to determine the similarity between primary biological sequence information, such as amino-acid sequences of proteins [44,45]. A high similarity in the genetic sequence indicates a high structural similarity. Due to the fact that three protein structures are either not available in the database or still unknown in their sequences, only five S-layer proteins were considered.

The following UniProt data were used:
L. sphaericus JG-A12 - Q5K102 (Q5K102_LYSSH),
L. sphaericus JG-B53 - M4N8T6 (M4N8T6_LYSSH),
L. sphaericus NCTC 9602 - Q5K104 (Q5K104_LYSSH),
S. ureae ATCC 13881 - Q3T908 (Q3T908_SPOUR),
G. stearothermophilus 12980 - P35825 (SLAP_GEOSE).

3. Results and discussion

3.1. Characterization of S-layer functionalized AuNP

The synthesized S-layer protein functionalized AuNP were characterized by TEM (Fig. 1) and UV/Vis spectroscopy (Fig. 2). Fig. 1 shows two examples of AuNP before and after functionalization with S-layer proteins. Particles without protein functionalization are typically characterized by a sharp border (Fig. 1(A)). In contrast, functionalized AuNP are surrounded by a homogenous corona of dark grey, representing the shell of appropriate S-layer proteins (Fig. 1(B), see also Supplementary information Fig. SI3), which are visualized by negative staining of the TEM samples with 2% uranyl acetate. According to the TEM analysis of the dried samples, the general thickness of all protein shells was 1–2 nm. Based on DLS measurements, however, a larger size of the native state of the protein shell in solution, which are covering the AuNP surface, can be assumed [17] (see also Supplementary information Fig. SI2). The difference in the visible size of the AuNP-biohybrids between TEM and DLS can be attributed to the different measurement principles. DLS represents the hydrodynamic diameter of the particles in solution, which is bigger than in the dried TEM samples.

Due to the fact that the plasmon resonance strongly depends on the dielectric environment, UV/Vis spectroscopy can be used to measure the protein adsorption of the biohybrid. As depicted in Fig. 2, the maximum of absorbance of the citrate capped AuNP, slightly shifted to a higher wavelength in the presence of S-layer proteins on the AuNP-surface. Typically, this shift was in a range of 4–5 nm. To ensure that no incorrect measurements of the biohybrid systems taken place, inadequate colloidal solutions that already started particle agglomeration indicated by peak broadening, shoulder, or additional peaks at higher wavelengths, where not used.

Altogether, the protein corona visualized by TEM, the peak shift at

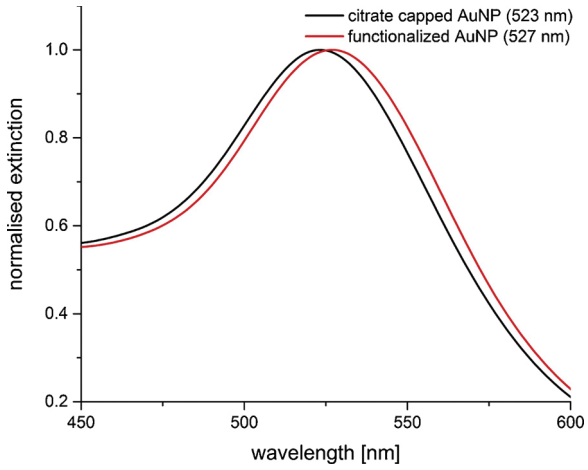

Fig. 2. UV/Vis spectra of citrate capped AuNP in water and AuNP functionalized with S-layer protein from *L. sphaericus* JG-B53.

specific UV–vis spectra and the stability of the functionalized AuNP against ionic-destabilization (describe in Materials and Methods section), prove the successful functionalization of the AuNP with the S-layer proteins. All tested S-layer proteins exhibited suitable properties for the biofunctionalization of AuNP under optimized conditions of stable pH and a suitable protein concentration.

3.2. Interactions of eight biohybrid S-layer-AuNP systems with different analytes

The unique potential of the eight biohybrid S-layer-AuNP systems to detect different metals and metalloid ions in an aqueous system was investigated by colorimetric assays. Accordingly, eight S-layer proteins from different bacteria species were used for the bio-functionalization of the AuNP.

Table 1 depicts an overview of the experimental matrix for each biohybrid system with one of the eleven assessed analytes. Blue colored columns visualize combinations of S-layer functionalized AuNP with a clear interaction with an analyte, e.g. a color change from red to blue. The red colored columns illustrate no reaction of the biohybrid with the corresponding analyte. From this representation, it can be seen only whether a significant reaction with the analyte is indicated (blue), but not that each of these reactions looks different, e.g. different concentration ranges, stronger/weaker peak shift, or a different reaction pattern. This will be specified in the next sections with taking an in-depth look at the different reactions.

All used S-layer proteins within this study were reactive at least with two of the examined analytes. Because of the numerous functional

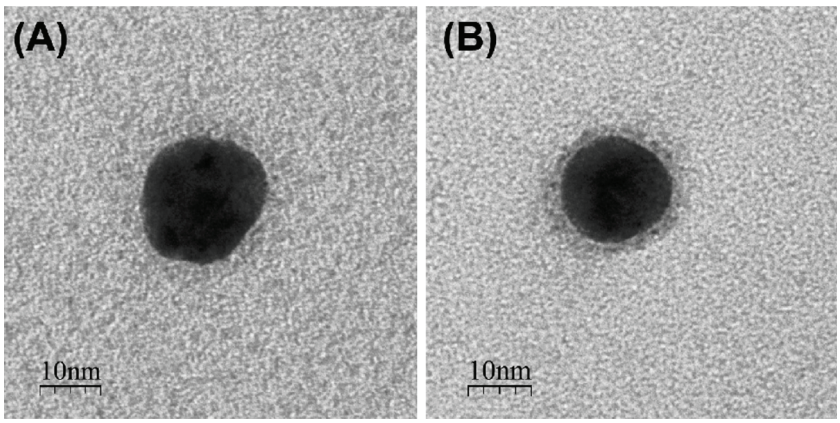

Fig. 1. TEM image of (A) a non-functionalized AuNP, and (B) a functionalized AuNP with Slp1 protein from *L. sphaericus* JG-B53.

Table 1
Schematic representation of the colorimetric reactions for eight different S-layer protein functionalized AuNP and the tested analytes. Blue signifies an interaction with the respective analyte, while the light red squares represent no detectable reaction. For *T. thermosulfurigenes* EM1 the value with As(V) is not available (n.a.). (For interpretation of the references to colour in this Table legend, the reader is referred to the web version of this article.).

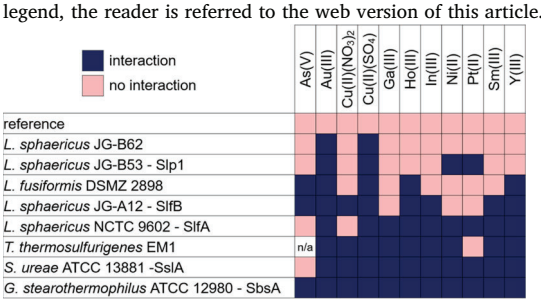

groups at the protein surface of the S-layers, such as NH_2, NH, OH, CO, COOH, SH and PO_4, this is no surprise, and resulted in a variety of interactions depending on the unique binding properties of the S-layer proteins. If those observed interactions between the multivalent positively charged analytes and the S-layers would have based on an unspecific electrostatic interaction, all of the results should finally show the same reaction. However, this was not the case. Therefore, the results in Table 1 supported our hypothesis of a specific interaction between the S-layers AuNP biohybrid system and analytes.

As expected, none of the utilized S-layer biohybrids responded identically for all analytes, as well as all biohybrid systems displayed different interaction behaviors depending on their S-layer and used analyte. Accordingly, if an S-layer-AuNP hybrid showed an interaction difference with at least two analytes, we examined and compared those differences to each other. For some analytes, several proteins displayed typical reactions, e.g. for Au(III), Cu(II)SO_4, Ho(III), Y(III) (see Table 1). Interestingly, all of our S-layer AuNP systems reacted with Au(III) and Cu(II)SO_4, despite their different amino acid sequences or structures, as assessed with UniProt. Therefore, it can be assumed that all of these S-layers must have at least one identical binding sites for these two analytes.

While Au(III) and Cu(II)SO_4 were detected by all eight tested S-layer-AuNP systems, the other analytes demonstrated reduced binding efficiency to at least three different S-layer-AuNP systems. It is also interesting to note that the two featuring different copper solutions, Cu(II)SO_4 and Cu(II)$(NO_3)_2$, were detected differently by four of the eight sensory active solutions.

Notable, the S-layer-AuNP system functionalized with the protein SbsA of *G. stearothermophilus* ATCC 12980 displayed reactions with all tested analyte solutions.

Interestingly, all biohybrid systems with the used four S-layer types of *L. sphaericus* species displayed different reaction patterns to the analytes. Here, we expected similarities in the reaction pattern due to their phylogenetic proximity. While the biohybrid system with the SlfA protein of *L. sphaericus* NCTC 9602 reacted with nine analytes, the one with *L. sphaericus* JG-B62 displayed a reaction with only two analytes. Within the tested S-layer-AuNP system, the one with protein SslA of *S. ureae* ATCC 13881 interacted with all chosen analytes, except As(V). The biohybrid system with the S-layer of *T. thermosulfurigenes* EM1 interacted with all analytes, except Pt(II). And finally, the S-layer of *L. fusiformis* DSMZ 2898 in the biohybrid system showed a reaction with As(V), Au(III), Cu(II)SO_4, Ho(III) and Y(III).

Due to the variety of the observed interaction patterns of the tested analytes with the S-layer biohybrid systems, the following two sections are addressed to further demonstrate the selectivity of the method. First, by the reaction of various S-layer proteins with only one specific analyte, and second for different reaction pattern of one S-layer biohybrid system with different analytes.

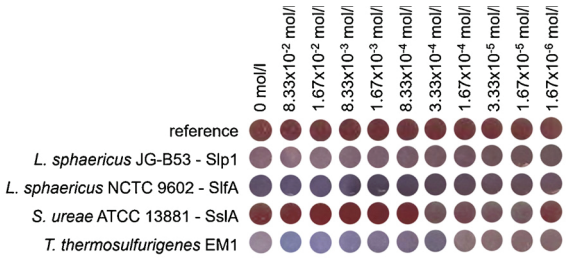

Fig. 3: Visible reaction pattern of the four S-layer-AuNP systems with varying concentrations of Y(III). Stable and weak reacting AuNP display red colors, while agglomerated and reactive AuNP are depicted in shades of blue.

Fig. 3. Visible reaction pattern of the four S-layer-AuNP systems with varying concentrations of Y(III). Stable and weak reacting AuNP display red colors, while agglomerated and reactive AuNP are depicted in shades of blue (For interpretation of the references to colour in this figure legend, the reader is referred to the web version of this article).

3.3. Detection of Y(III) by using four S-layer-AuNP systems

Fig. 3 gives a summary of the results for the colorimetric detection of Y(III) by four different S-layer biohybrids. AuNP stabilized with 0.1% PVA are used for reference.

The S-layer-AuNP system functionalized with Slp1 of *L. sphaericus* JG-B53 displayed no reactions at all tested Y(III) concentrations. The remaining three biohybrid systems showed different reaction patterns in different concentration ranges of Y(III). The S-layer-AuNP system functionalized with slfA protein showed a color change from red to blue, beginning at a concentration of 8.33×10^{-4} mol/l up to 8.33×10^{-2} mol/l Y(III). The SslA-functionalized biohybrid AuNP system displayed a reaction with Y(III) in a range between 1.67×10^{-5} mol/l and 3.33×10^{-4} mol/l. In the last case of AuNP functionalized with the S-layer protein of *T. thermosulfurigenes* EM1, the color changed from red to blue from 3.33×10^{-4} mol/l up to 8.33×10^{-2} mol/l. The accompanying specific reactions of the different S-layer AuNP systems with defined concentration ranges of an analyte depict the possibility to selectively distinguish an analyte by its color / absorbance shift. Utilizing a dilution series of the sample, the presence and also the concentration of a single metal ion can be determined by comparing the results with known reaction patterns as shown in Fig. 3. Due to the visible color change during the reaction, and therefore the detection of an analyte within some minutes, the method can easily be transferred to field measurements.

However, the biohybrid AuNP system with SslA protein showed a weak visual response that was perceivable by the eye. This outcome represents good example of the limitations of the system, thus heightening the need for additional evaluation methods, such as UV/Vis measurements, to get more detailed information about the sample and concentration range. Accordingly, Fig. 4 displays the UV/Vis spectra for the above-mentioned conditions of SslA AuNP system interacting with Y(III) within an estimated concentration range between 1.67×10^{-6} mol/l. till $\times 10^{-2}$ mol/l. The reference without Y(III) ions showed an absorption peak at 525 nm, whereas no peak shift was visible at a concentration of 1.67×10^{-6} mol/l Y(III). With increasing concentration of Y(III), the shift of the absorption peak to higher wavelengths became more pronounced, up to the strongest shift to 562 nm at a concentration of 1.67×10^{-4}mol/l Y(III).

As previously mentioned, the shift of the plasmon resonance occurred from the agglomeration of functionalized AuNP while interacting with the analyte (see Fig. SI4 in Supplementary information). At higher concentration, the peak shifts back to smaller wavelengths with a maximum at 534 nm. This smaller shift results from a saturation of the binding sites of the S-layer by the increased Y(III) ion concentration. The saturation leads to less cross-linkage, because there are less free binding sites available, and therefore results in the formation of minor

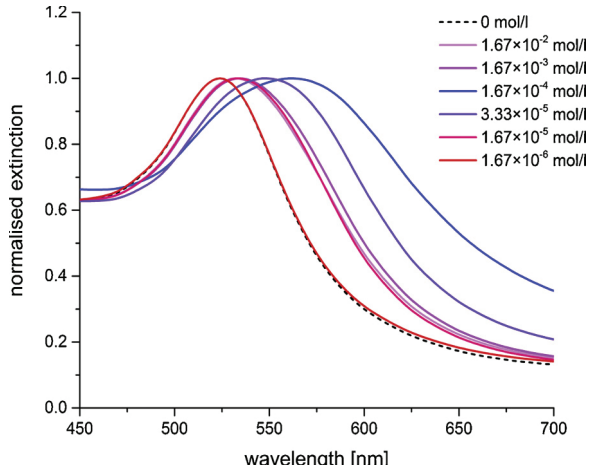

Fig. 4. UV/Vis spectra of SslA AuNP system with protein from *S. ureae* ATCC 13881 treated with different concentrations of Y(III).

agglomerates.

In order to obtain a clear presentation of the data and to enable a better comparability of the different reaction patterns of the tested S-layer-AuNP systems, the results of the UV/Vis measurements can be reduced to the absorbance at 575 nm.

Fig. 5 illustrates those relative changes of the extinction at 575 nm for different Y(III) concentration. The extinction of the reference was subtracted from the measured value at the same wavelength, resulting in a percentage based demonstration of the different S-layer AuNP systems according to the different Y(III) concentration (see Equation 1 in Supplementary Information). The resulting curves now can be plotted against the YCl_3 concentration, compared more easily and the difference in reaction ranges and reaction patterns can be extracted.

The biohybrid AuNP system functionalized with Slp1 of *L. sphaericus* JG-B53 showed no reaction at all tested Y(III) concentrations. In contrast, the biohybrid AuNP system functionalized with SlfA showed an increase in the relative extinction at 575 nm, beginning with 8.33×10^{-4} mol/l up to 8.33×10^{-2} mol/l, with a maximum of 25.92 ± 5.87% at 1.67×10^{-3} mol/l Y(III). The SslA-AuNP system displayed a strong change of the extinction in a range between 1.67×10^{-5} mol/l and 3.33×10^{-4} mol/l with the maximum extinction change of 118.12 ± 4.82% at 3.33×10^{-4} mol/l. Finally, for the S-layer protein of *T. thermosulfurigenes* EM1 the relative extinction change ranged from 3.33×10^{-4} mol/l up to 8.33×10^{-2} mol/l, with the strongest signal of 121.81 ± 7.58% at 3.33×10^{-4} mol/l.

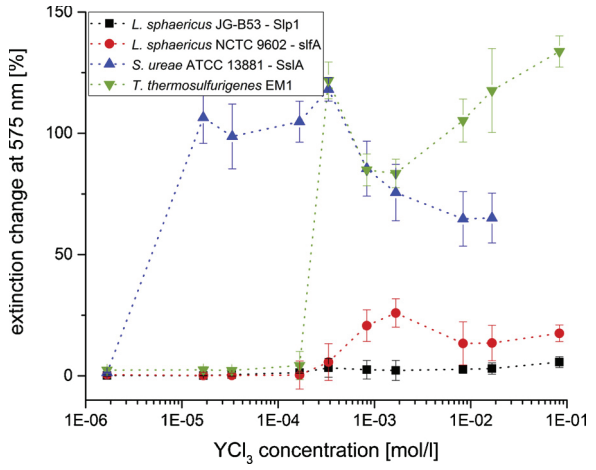

Fig. 5. Relative extinction change at 575 nm of four different bio-hybrid AuNP systems in interaction with YCl_3.

Additionally, different reaction patterns of the S-layer-AuNP systems were shown and can be distinguished at an extinction at 575 nm.

Visually, the reactions of the S-layer-AuNP systems functionalized with SlfA or with the S-layer of *T. thermosulfurigenes* EM1 were in a similar concentration range, which can be simplified by using the extinction at 575 nm. The simple specific differentiation therein, which of the two S-layer proteins has interacted in particular with the Y(III) dilution series, can be distinguished. According to those experiments, the example SslA-AuNP system showed the lowest detection limit for Y(III) at 1.67×10^{-5}mol/l for all the used experiments within this study.

Here, we were able to describe the selectivity of several S-layer functionalized AuNP hybrids, for one specific analyte.

3.4. Reactivity of the biohybrid AuNP system functionalized with SslA protein with Au(III), Ho(III), In(III) and Y(III)

Next, the selectivity of one S-layer-AuNP system for several analytes will be defined. Therefore, the previously described SsIA functionalized AuNP system, and the analytes Au(III), Ho(III), In(III), as well as Y(III) were used. When examining the interactions of this one S-layer-AuNP system with the various analytes, the color shift visually was partly similar from red to blue. As discussed previously, the results of UV/Vis measurements allow more nuanced findings, than the detection with the eyes. Therefore, the values of the calculations from the relative change of extinction at 575 nm were plotted against the corresponding metal or metalloid ion concentration (Fig. 6). The graphs show different reaction patterns depending on the type of metal or metalloid ion (see also Fig. SI6 in Supplementary information).

For the biohybrid AuNP system functionalized with SslA, the lowest detection limit of 3.33×10^{-6}mol/l was measured for Au(III) with the strongest extinction change with 100.63 ± 16.33%. By increasing the analyte concentration, the extinction initially decreased to about half with 53.68 ± 4.12%, prior of a new rising up to 102.72 ± 0.11% at a concentration of 1.67×10^{-2}mol/l. No extinction changes was assessable at the lowest measured Au(III) concentration of 1.67×10^{-6}mol/l (5.21 ± 1.22%).

For Ho(III) and Y(III), the SslA functionalized AuNP system showed similar reaction patterns. The detection limits were measured between 1.67×10^{-6}mol/l and 1.67×10^{-5}mol/l, respectively, with the strongest changes of extinction between 3.33×10^{-5}mol/l and 1.67×10^{-4}mol/l. At higher concentrations, the signal decreased to 50–60 %. The similarity in the reaction patterns for Ho(III) and Y(III) indicated an analogous binding mechanism of SslA protein with both elements.

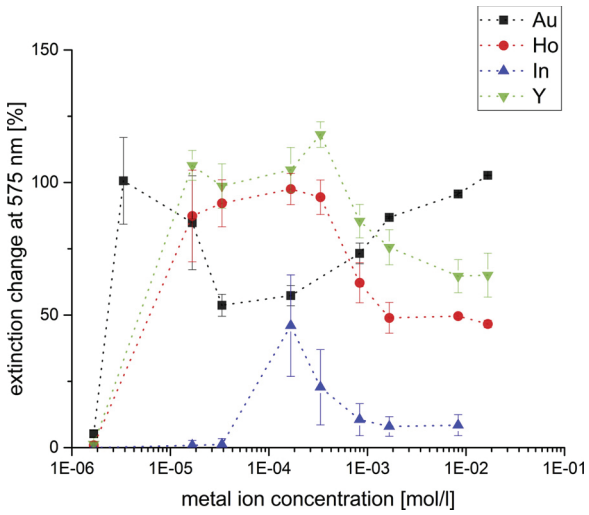

Fig. 6. Relative extinction change at 575 nm of bio-hybrid AuNP system functionalized with SslA protein from *S. ureae* ATCC 13881 in interaction with different analytes in various concentrations indicated in the legend.

Table 2
Sequence identity data from protein BLAST of five S-layer proteins. Green indicates high sequence identity, and red low sequence identity. (For interpretation of the references to colour in this Table legend, the reader is referred to the web version of this article.).

	SlfB	Slp1	SlfA	SslA	SbsA
L. sphaericus JG-A12 - SlfB		67%	79%	52%	28%
L. sphaericus JG-B53 - Slp1	67%		65%	52%	31%
L. sphaericus NCTC 9602 - SlfA	79%	65%		48%	54%
S. ureae ATCC 13881 - SslA	52%	52%	48%		58%
G. stearothermophilus ATCC 12980 - SbsA	28%	31%	54%	58%	

Here, the available reactive groups of the S-layer surface might interact with the analytes by forming novel binding sites, which seems to be similar for Ho(III) and Y(III) as evidenced by their comparable reaction patterns.

In general, the differences in the interaction pattern can be used to specifiy the present metal ions of a sample. Further, as shown in Fig. 6, the specific extinction curves (see Fig. SI6 in Supplementary information), together with a dilution series of the sample, might determine the unknown concentration of a sample with known metal ions. By testing a sample with multiple S-layer-AuNP systems, a distinction between multiple ions in solution via colorimetric assay would be possible.

However, this approach to develop a screening assay has to be investigated in further experiments, especially with regard to cross-reactivity in the presence of different analytes. These findings could be a starting point for the development of a fast and simple screening assay for different analytes. However, it has to be stated, that the system is influenced by complex parameters and not yet optimized. Since the system is not buffered, the influence of different pH values has to be investigated further in detail. Moreover, the effect of different anions as well as the respective present ionic species in general has to be elucidated.

3.5. Sequence comparison of S-layer proteins SlfB, Slp1, SlfA, SslA and SbsA

The variability in the reaction of the S-layer proteins to the appropriate analytes demonstrated that S-layer represent interesting exploration objects. It is of great interest to correlate these results precisely to their biological phylogeny and sequence. Pollmann et al. [9] described a high similarity between the S-layer protein SlfB (*L. sphaericus* JG-A12) and SlfA (*L. sphaericus* NCTC 9602), with 98% sequence identity and a difference of only 3 amino acids / 13 nucleotides [46,47]. Similarly, Lederer et al. [48] compared Slp1 (*L. sphaericus* JG-B53) to SlfB with a 67% sequence identity, as well as 65% for Slp1 to SlfA sequence identity.

Differences between the literature and our results can be explained by the different used software for sequence comparison, as well as the used version.Despite this fact that the protein BLAST results showed differing values for the sequence identity, the highest sequence identity values (79%) were evaluated for both SlfB and SlfA (Table 2). Additionally, the three S-layer proteins SlfA, SlfB and Slp1 from the same species *L. sphaericus* demonstrated high sequence identities between SlfB and SlfA, and for SlfB and Slp1.

It should also be noted that even though SlfA and SlfB display high sequence identity, they reacted very differently with metal and metalloid ions. Therefore, the hypothesis of similar amino acid sequences leading to comparable binding properties for those proteins might be rejectable. The fact that based on the amino acid sequence, it is not possible to define the binding pattern of the S-layer proteins confirms that their specific binding affinities must be experimental determined more intensively. In the experimental design, additional influencing factors, such as the pH value, must be taken into account. This in turn affects the net charge of the proteins and the chemical speciation of the analytes. Studies have already shown differences in the growth conditions of the bacteria can lead to post-translational modifications of S-layer proteins [49]. These post-translational protein modifications might also influence binding properties. Recently, Lederer et al. (2013) recently described various environmental factors that could impact the binding capacity of S-layer proteins [48]. In particular, the authors noted that cells can present different S-layer variants with specific abilities to cope with fast-changing environmental conditions.

4. Conclusions

The herein described results represent one of the most extensive studies for the colorimetric detection of different analytes with S-layer protein-functionalized AuNP. Eleven different analytes, including the rare-earth elements Ho(III), Sm(III), and Y(III), as well as noble metal complexes such as Au(II), and Pt(II); as well as the toxic element As(V), were analyzed by our established colorimetric biohybrid assays. Especially for the rare-earth elements, to-date there are only a limited number of analytic methods available.

In our experimental setting, the typical colorimetric reaction was confirmed visually by a color shift from red to blue. The detection threshold of our method was improved by UV/Vis measurements and a wavelength dependent correlation method. For the major example described in our study, a highly specific detection of Y(III) up to a concentration of 1.67×10^{-5} mol/l was achieved for the SslA-AuNP system.

Furthermore, our data verified a unique reaction pattern for each of the verified S-layer-AuNP hybrid systems with all tested analytes, facilitating the specific detection of metal and metalloid ions in an aqueous solution. First attempts to correlate the binding mechanisms of the S-layer and the analytes to the specific sequence identity data of the S-layers, indicated that the interaction capability not only depends on the amino acid sequence, but also on essential environmental or epigenetic factors.

The colorimetric biohybrid system described herein can be established as a rapid and easy screening assay for the tested rare-earth elements as well as expanded to other metal ions.

Declaration of Competing Interest

There are no conflicts of interest to declare.

Acknowledgements

We thank Beate Katzschner for supporting the preparation of S-layer proteins, and Phil Goldberg for providing an external point of view and in-depth discussion. This research has been funded by the Bundesministerium für Bildung und Forschung (BMBF, 03WKCL03D) and European Social Fund (ESF, 100284305).

Appendix A. Supplementary data

References

[1] S. Schultze-Lam, T.J. Beveridge, Nucleation of celestite and strontianite on a cyanobacterial S-layer, Appl. Environ. Microbiol. 60 (1994) 447–453.

[2] V.R. Phoenix, R.W. Renaut, B. Jones, F.G. Ferris, Bacterial S-layer preservation and rare arsenic–antimony–sulphide bioimmobilization in siliceous sediments from Champagne Pool hot spring, Waiotapu, New Zealand, J. Geol. Soc. Lond. 162 (2005) 323–331, https://doi.org/10.1144/0016-764903-058.

[3] M.C. Allievi, S. Florencia, P.A. Mariano, P.M. Mercedes, S.M. Ruzal, S.R. Carmen, Metal biosorption by surface-layer proteins from Bacillus species, J. Microbiol. Biotechnol. 21 (2011) 147–153 https://doi.org/10.4014/jmb.1009.09046.

[4] E. Gerbino, P. Carasi, P. Mobili, M.A. Serradell, A. Gómez-Zavaglia, Role of S-layer proteins in bacteria, World J. Microbiol. Biotechnol. 31 (2015) 1877–1887, https://doi.org/10.1007/s11274-015-1952-9.

[5] U.B. Sleytr, T.J. Beveridge, Bacterial S-layers, Trends Microbiol. 7 (1999) 253–260, https://doi.org/10.1016/S0966-842X(99)01513-9.

[6] M. Sára, U.B. Sleytr, S-layer proteins, J. Bacteriol. 182 (2000) 859–868, https://doi.org/10.1128/JB.182.4.859-868.2000.

[7] S. Selenska-Pobell, P. Panak, V. Miteva, I. Boudakov, G. Bernhard, H. Nitsche, Selective accumulation of heavy metals by three indigenous {Bacillus} strains, {B}-cereus, {B}-megaterium and {B}-sphaericus, from drain waters of a uranium waste pile, FEMS Microbiol. Ecol. 29 (1999) 59–67 //000080187400006.

[8] J. Raff, U. Soltmann, S. Matys, S. Selenska-Pobell, H. Böttcher, W. Pompe, Biosorption of uranium and copper by biocers, Chem. Mater. 15 (2003) 240–244, https://doi.org/10.1021/cm021213l.

[9] K. Pollmann, J. Raff, M. Merroun, K. Fahmy, S. Selenska-Pobell, Metal binding by bacteria from uranium mining waste piles and its technological applications, Biotechnol. Adv. 24 (2006) 58–68, https://doi.org/10.1016/j.biotechadv.2005.06.002.

[10] M. Suhr, N. Unger, K.E. Viacava, T.J. Günther, J. Raff, K. Pollmann, Investigation of metal sorption behavior of Slp1 from Lysinibacillus sphaericus JG-B53: a combined study using QCM-D, ICP-MS and AFM, Biometals 27 (2014) 1337–1349, https://doi.org/10.1007/s10534-014-9794-8.

[11] U.B. Sleytr, P. Messner, D. Pum, M. Sara, Crystalline bacterial cell surface layers: general principles and application potential, Mol. Microbiol. 10 (1993) 911–916, https://doi.org/10.1111/j.1365-2672.1993.tb04339.x.

[12] U.B. Sleytr, H. Bayley, M. Sára, A. Breitwieser, S. Küpcü, C. Mader, S. Weigert, F.M. Unger, P. Messner, B. Jahn-Schmid, B. Schuster, D. Pum, K. Douglas, N.A. Clark, J.T. Moore, T.A. Winningham, S. Levy, I. Frithsen, J. Pankovc, P. Beale, H.P. Gillis, D.A. Choutov, K.P. Martin, VI. Applications of S-layers, FEMS Microbiol. Rev. 20 (1997) 151–175, https://doi.org/10.1016/S0168-6445(97)00044-2.

[13] W. Shenton, D. Pum, U.B. Sleytr, S. Mann, Synthesis of cadmium sulphide superlattices using self-assembled bacterial S-layers, Nature 389 (1997) 585–587, https://doi.org/10.1038/39287.

[14] U.B. Sleytr, C. Huber, N. Ilk, D. Pum, B. Schuster, E.M. Egelseer, S-layers as a tool kit for nanobiotechnological applications, FEMS Microbiol. Lett. 267 (2007) 131–144, https://doi.org/10.1111/j.1574-6968.2006.00573.x.

[15] U.B. Sleytr, B. Schuster, E.M. Egelseer, D. Pum, S-layers: principles and applications, FEMS Microbiol. Rev. 38 (2014) 823–864, https://doi.org/10.1111/1574-6976.12063.

[16] K. Pollmann, S. Kutschke, S. Matys, S. Kostudis, S. Hopfe, J. Raff, Novel biotechnological approaches for the recovery of metals from primary and secondary resources, Minerals 6 (2016) 54, https://doi.org/10.3390/min6020054.

[17] M. Lakatos, S. Matys, J. Raff, W. Pompe, Colorimetric as (V) detection based on S-layer functionalized gold nanoparticles, Talanta 144 (2015) 241–246, https://doi.org/10.1016/j.talanta.2015.05.082.

[18] M. Zhuang, J. Zhao, S. Li, D. Liu, K. Wang, P. Xiao, L. Yu, Y. Jiang, J. Song, J. Zhou, L. Wang, Z. Chu, M. Zhuang, J. Zhao, S. Li, D. Liu, K. Wang, P. Xiao, L. Yu, Y. Jiang, J. Song, J. Zhou, L. Wang, Z. Chu, M. Zhuang, J. Zhao, S. Li, D. Liu, K. Wang, P. Xiao, L. Yu, Y. Jiang, J. Song, J. Zhou, L. Wang, Z. Chu, Concentrations and health risk assessment of rare earth elements in vegetables from mining area in Shandong, China, Chemosphere 168 (2017) 578–582, https://doi.org/10.1016/j.chemosphere.2016.11.023.

[19] K.M. Goodenough, F. Wall, D. Merriman, The rare earth elements: demand, global resources, and challenges for resourcing future generations, Nat. Resour. Res. 27 (2018) 201–216, https://doi.org/10.1007/s11053-017-9336-5.

[20] J.O. Duruibe, M.O. Ogwuegbu, J.N. Egwurugwu, Heavy metal pollution and human biotoxic effects, Int. J. Phys. Sci. 2 (2007) 112–118, https://doi.org/10.1016/j.proenv.2011.09.146.

[21] L.M. Jakubek, S. Marangoudakis, J. Raingo, X. Liu, D. Lipscombe, R.H. Hurt, The inhibition of neuronal calcium ion channels by trace levels of yttrium released from carbon nanotubes, Biomaterials 30 (2009) 6351–6357, https://doi.org/10.1016/j.biomaterials.2009.08.009.

[22] P.C. Nagajyoti, K.D. Lee, T.V.M. Sreekanth, Heavy metals, occurrence and toxicity for plants: a review, Environ. Chem. Lett. 8 (2010) 199–216, https://doi.org/10.1007/s10311-010-0297-8.

[23] Z. Li, Z. Ma, T.J. van der Kuijp, Z. Yuan, L. Huang, A review of soil heavy metal pollution from mines in China: pollution and health risk assessment, Sci. Total Environ. 468–469 (2014) 843–853, https://doi.org/10.1016/j.scitotenv.2013.08.090.

[24] B. Wei, L. Yang, A review of heavy metal contaminations in urban soils, urban road dusts and agricultural soils from China, Microchem. J. 94 (2010) 99–107, https://doi.org/10.1016/j.microc.2009.09.014.

[25] S. Audry, J. Schäfer, G. Blanc, J.M. Jouanneau, Fifty-year sedimentary record of heavy metal pollution (Cd, Zn, Cu, Pb) in the Lot River reservoirs (France), Environ. Pollut. 132 (2004) 413–426, https://doi.org/10.1016/j.envpol.2004.05.025.

[26] F. Sulotto, C. Romano, A. Berra, G.C. Botta, G.F. Rubino, E. Sabbioni, R. Pietra, Rare earth pneumoconiosis: a new case, Am. J. Ind. Med. 9 (1986) 567–575, https://doi.org/10.1002/ajim.4700090609.

[27] D.L. Tomlinson, J.G. Wilson, C.R. Harris, D.W. Jeffrey, Problems in the assessment of heavy-metal levels in estuaries and the formation of a pollution index, Helgoländer Meeresunters. 33 (1980) 566–575, https://doi.org/10.1007/BF02414780.

[28] J.F. Boissonneau, M.J. Repellin, A. Eglem, Elecrochemical detection of rare earths and yttrium after chromatographic separation by high performance liquid chromatography, Analusis 8 (1980) 230–237.

[29] K. Yoshida, H. Haraguchi, Determination of rare earth elements by liquid chromatography/inductively coupled plasma atomic emission, Anal. Chem. 56 (1984) 2580–2585, https://doi.org/10.1021/ac00277a069.

[30] P.L. Smedley, The geochemistry of rare earth elements in groundwater from the Carnmenellis area, southwest England, Geochim. Cosmochim. Acta 55 (1991) 2767–2779, https://doi.org/10.1016/0016-7037(91)90443-9.

[31] K. Benkhedda, H. Goenaga Infante, E. Ivanova, F.C. Adams, Determination of sub-parts-per-trillion levels of rare earth elements in natural waters by inductively coupled plasma time-of-flight mass spectrometry after flow injection on-line sorption preconcentration in a knotted reactor, J. Anal. At. Spectrom. 16 (2001) 995–1001, https://doi.org/10.1039/b101343m.

[32] D.W. Hicklin, W.M. Willingham, Evaluation of Commercially Available Cyanide Test Kits Against Various Matrices, (2016).

[33] E. Ruiz-Hitzky, M. Darder, P. Aranda, K. Ariga, Advances in biomimetic and nanostructured biohybrid materials, Adv. Mater. 22 (2010) 323–336, https://doi.org/10.1002/adma.200901134.

[34] J. Turkevich, P.C. Stevenson, J. Hillier, A study of the nucleation and growth processes I N the synthesis of colloidal gold, Discuss. Faraday Soc. 11 (1951) 55–75.

[35] G. Frens, Controlled nucleation for the regulation of the particle size in monodisperse gold suspensions, Nat. Phys. Sci. 241 (1973).

[36] A. Blüher, K. Ostermann, P. Jäckel, A. Clemens, B. Katzschner, G. Rödel, M. Mertig, Extraction and long-term storage of S-layer proteins and flagella from Lysinibacillus sphaericus NCTC 9602: building blocks for nanotechnology, Eng. Life Sci. 15 (2015) 410–415, https://doi.org/10.1002/elsc.201400182.

[37] E. Brechtel, M. Matuschek, A. Hellberg, E.M. Egelseer, R. Schmid, H. Bahl, Cell wall of thermoanaerobacterium thermosulfurigenes EM1: isolation of its components and attachment of the xylanase XynA, Arch. Microbiol. 171 (1999) 159–165, https://doi.org/10.1007/s002030050694.

[38] D. Fritze, Taxonomy of the genus *Bacillus* and related genera: the aerobic endospore-forming bacteria, Phytopathology 94 (2004) 1245–1248, https://doi.org/10.1094/PHYTO.2004.94.11.1245.

[39] W.D. Geoghegan, G.A. Ackerman, Adsorption of horseradish ovomucoid and anti-immunoglobulin to colloidal for the indirect detection of concanavalin a, wheat germ anti- G on cell surfaces at the electron microscopic level: a new method, theory and application, J. Histochem. Cytochem. 25 (1977) 1187–1200.

[40] I. Horcas, R. Fernández, J.M. Gómez-Rodríguez, J. Colchero, J. Gómez-Herrero, A.M. Baro, WSXM: a software for scanning probe microscopy and a tool for nanotechnology, Rev. Sci. Instrum. 78 (2007), https://doi.org/10.1063/1.2432410.

[41] U. Hinz, From protein sequences to 3D-structures and beyond: the example of the UniProt Knowledgebase, Cell. Mol. Life Sci. 67 (2010) 1049–1064, https://doi.org/10.1007/s00018-009-0229-6.

[42] The UniProt Consortium, UniProt Database. http://www.uniprot.org (Accessed 1 September 2017).

[43] UniProt Consortium, UniProt: a hub for protein information, Nucleic Acids Res. 43 (2015) D204–D212, https://doi.org/10.1093/nar/gku989.

[44] National Center for Biotechnology Information, U.S. National Library of Medicine, NCBI Protein Basic Local Alignment Search Tool – BLAST. https://blast.ncbi.nlm.nih.gov/Blast.cgi?PROGRAM=blastp&PAGE_TYPE=BlastSearch&LINK_LOC=blasthome (Accessed 1 September 2017).

[45] S.F. Altschul, W. Gish, W. Miller, E.W. Myers, D.J. Lipman, Basic local alignment search tool, J. Mol. Biol. 215 (1990) 403–410, https://doi.org/10.1016/S0022-2836(05)80360-2.

[46] K. Pollmann, J. Raff, M. Schnorpfeil, G. Radeva, S. Selenska-Pobell, Novel surface layer protein genes in Bacillus sphaericus associated with unusual insertion elements, Microbiology 151 (2005) 2961–2973, https://doi.org/10.1099/mic.0.28201-0.

[47] K. Pollmann, S. Matys, Construction of an S-layer protein exhibiting modified self-assembling properties and enhanced metal binding capacities, Appl. Microbiol. Biotechnol. 75 (2007) 1079–1085, https://doi.org/10.1007/s00253-007-0937-5.

[48] F.L. Lederer, U. Weinert, T.J. Günther, J. Raff, S. Weiß, K. Pollmann, Identification of multiple putative S-layer genes partly expressed by Lysinibacillus sphaericus JG-B53, Microbiology (United Kingdom) 159 (2013) 1097–1108, https://doi.org/10.1099/mic.0.065763-0.

[49] Z. Guan, S. Naparstek, D. Calo, J. Eichler, Protein glycosylation as an adaptive response in archaea: growth at different salt concentrations leads to alterations in Haloferax volcanii S-layer glycoprotein N-glycosylation, Environ. Microbiol. 14 (2012) 743–753, https://doi.org/10.1111/j.1462-2920.2011.02625.x.